Chapter 2

Radar polarimetry

Although the foundational ideas of radar polarimetry date back to the 1970s and can be considered a mature concept – with the 1980s and 1990s representing a golden period of theoretical and experimental development for synthetic aperture radar (SAR) and meteorology [1] – its application potential in the automotive industry began to emerge only in the previous decade. In remote sensing, polarimetry has long been the standard for classifying terrain textures or hydrometeor shapes; however, transferring these techniques to the automotive domain presents unique challenges. Unlike the far-field, high-altitude geometries of SAR, automotive radar operates at grazing incidence angles with significant multipath interaction, in the near-to-intermediate field, and against highly dynamic, non-cooperative targets.

Consequently, the field of polarimetric automotive radar remains in its infancy, lacking robust methods for classifying dynamic vulnerable road users (VRUs) such as pedestrians and cyclists. Nonetheless, it holds a compelling promise for achieving higher reliability and sophistication in sensors for advanced driver-assistance systems (ADAS) and autonomous driving. This promise has captured the attention of major automotive companies and research institutes, prompting viability confirmations [2] and proof-of-concept system implementations [3]. The rapidly increasing innovation in this area is further evidenced by the recent emergence of monographs focusing specifically on polarimetric radar for automotive applications [4].

Establishing a polarimetric framework for VRU classification, however, places stringent demands on the underlying radar architecture. The theoretical requirements for high polarization purity and cross-polarization discrimination (XPD) directly inform the selection of radiating element types and feeding integration platforms, as will be discussed in detail in Chapter 3. Furthermore, the need for simultaneous acquisition of the full scattering matrix for dynamic scenes necessitates a sophisticated large-aperture MIMO configuration. The design of this MIMO topology and its impact on virtual aperture and polarimetric diversity will be the focus of Chapter 4. This introductory chapter therefore provides the theoretical and phenomenological motivation for the hardware and topological developments that follow.

The exposition given in this chapter follows standard references to electrodynamics and radar polarimetry, such as Zangwill [5] and Lee and Pottier [1], respectively. Additionally, a specialized monograph on polarimetric radar for automotive applications by Visentin [4], is discussed to provide further context and detail.

Add citations throughout the chapter.

2.1 Fundamentals of radar polarimetry

Electromagnetic waves can be decomposed into orthogonal linear, circular, or elliptical polarization states, each associated with a specific temporal evolution of the electric field vector. In radar applications, polarization serves as an additional dimension for characterizing scattering mechanisms: targets may preserve, transform, or depolarize the incident wave depending on their geometry, surface material, roughness, and orientation. These transformations provide valuable

classification features that are absent in scalar radar measurements [1].

The description of polarization typically relies on the Jones vector for coherent fields and the Stokes vector or coherency matrix for partially coherent and incoherent fields. At automotive millimetre-wave frequencies, the high coherence of FMCW radars allows Jones and coherency representations to remain applicable. The polarization purity of the transmitted and received waves, however, is strongly influenced by antenna cross-polarization discrimination (XPD), PCB anisotropies, and mutual coupling – highlighting the need for the careful array design discussed in Chapter 3.

Time convention. As common in engineering monographs, this text treats the convention of time as *positive*, meaning that a scalar wave $w(\xi, t)$ propagating in the ξ direction is expressed as $\exp[\mathrm{i}(\omega t - k\xi)]$. This is in contrast to physics literature, which often adopts a *negative time* convention, leading to $\exp[\mathrm{i}(k\xi - \omega t)]$.

2.1.1 Polarization of electromagnetic waves

While the full propagation of electromagnetic energy is governed by Maxwell's equations, for radar polarimetry it suffices to consider the solution for a monochromatic plane wave propagating in a direction given by the wave vector $\boldsymbol{k} = k\boldsymbol{e}_k$ with angular frequency $\omega = 2\pi f$. Such electric and magnetic vector fields can be expressed as

$$\boldsymbol{E}(\boldsymbol{r}, t) = \boldsymbol{\mathcal{E}}_\perp \exp[\mathrm{i}(\omega t - \boldsymbol{k}\cdot\boldsymbol{r})] \qquad \text{and} \qquad \boldsymbol{B}(\boldsymbol{r}, t) = \boldsymbol{\mathcal{B}}_\perp \exp[\mathrm{i}(\omega t - \boldsymbol{k}\cdot\boldsymbol{r})]\,, \tag{2.1}$$

where $\boldsymbol{\mathcal{E}}_\perp$ and $c\boldsymbol{\mathcal{B}}_\perp = \boldsymbol{e}_k \times \boldsymbol{\mathcal{E}}_\perp$ are generally complex amplitude vectors perpendicular to the direction of propagation. The physical fields of a monochromatic plane wave are the *real parts* of these expressions. Focusing on the electric field component, we have

$$\boldsymbol{E}(\boldsymbol{r}, t) = \begin{bmatrix} |E_H| \exp(\mathrm{i}\delta_H) \\ |E_V| \exp(\mathrm{i}\delta_V) \end{bmatrix} \exp[\mathrm{i}(\omega t - kz)]\,, \tag{2.2}$$

where δ_H and δ_V denote the phase offsets of the horizontal and vertical components, respectively. The choice of the transverse basis vectors is arbitrary; however, in radar applications, it is customary to select orthogonal basis vectors perpendicular to the direction of propagation, horizontal (H) and vertical (V).

The polarization state – the geometric locus traced by the tip of the electric field vector over time – is fully described by the Jones vector $\boldsymbol{E}_J$. For a fully coherent wave, the *Jones vector* is defined by the amplitudes $|E_H|$ and $|E_V|$ and the relative phase difference $\delta = \delta_V - \delta_H$:

$$\boldsymbol{E}_J = \begin{bmatrix} E_H \\ E_V \end{bmatrix} = \begin{bmatrix} |E_H| \mathrm{e}^{\mathrm{i}\delta_H} \\ |E_V| \mathrm{e}^{\mathrm{i}\delta_V} \end{bmatrix} = \mathrm{e}^{\mathrm{i}\delta_H} \begin{bmatrix} |E_H| \\ |E_V| \mathrm{e}^{\mathrm{i}\delta} \end{bmatrix}. \tag{2.3}$$

This representation is critical for the MIMO system design discussed in Chapter 4, as the transmitter and receiver chains operate coherently. However, the Jones vector is strictly valid only for fully polarized, monochromatic waves.

2.1.2 The Sinclair scattering matrix

When concerned with scattering off targets, the relationship between the incident and scattered electric fields is of primary interest. As discussed in the previous sections, polarization of a monochromatic plane wave at a given instant can be fully characterized by the Jones vector. Furthermore, a set of two orthogonal Jones vectors forms a polarization basis. Therefore, it is possible to establish a linear scattering model that relates the incident and scattered Jones

vectors, $\boldsymbol{E}_{\text{in}}$ and $\boldsymbol{E}_{\text{sc}}$, respectively, via a complex scattering matrix:[1]

$$\boldsymbol{E}_{\text{sc}} = \frac{\mathrm{e}^{-\mathrm{i}kr}}{r}\boldsymbol{S}\boldsymbol{E}_{\text{in}} = \frac{\mathrm{e}^{-\mathrm{i}kr}}{r}\begin{bmatrix} S_{\text{HH}} & S_{\text{HV}} \\ S_{\text{VH}} & S_{\text{VV}} \end{bmatrix}\boldsymbol{E}_{\text{in}}. \tag{2.4}$$

The matrix $\boldsymbol{S}$, called the *Sinclair scattering matrix*, encapsulates the target's polarimetric response, with each element S_{pq} representing the complex scattering amplitude from transmit polarization p to receive polarization q. The diagonal terms are often called *co-polar* components, while the off-diagonal terms are referred to as *cross-polar* components. Furthermore, under the assumption of reciprocity in a linear, time-invariant medium, the scattering matrix is symmetric, yielding

$$\boldsymbol{S} = \exp(\mathrm{i}\phi_{\text{HH}})\begin{bmatrix} |S_{\text{HH}}| & |S_{\text{HV}}|\exp\left[\mathrm{i}(\phi_{\text{HV}} - \phi_{\text{HH}})\right] \\ |S_{\text{HV}}|\exp\left[\mathrm{i}(\phi_{\text{HV}} - \phi_{\text{HH}})\right] & |S_{\text{VV}}|\exp\left[\mathrm{i}(\phi_{\text{VV}} - \phi_{\text{HH}})\right] \end{bmatrix}. \tag{2.5}$$

The absolute phase term $\exp(\mathrm{i}\phi_{\text{HH}})$ is not considered an independent parameter since it represents an arbitrary value given by the target range. The main consequence of this symmetry is a reduction in the number of independent parameters from eight to five.[2] However, practical considerations in automotive radar often challenge this ideal model by introducing near-field effects: Reciprocity holds for plane waves; for targets in the near-field of the array, such as a pedestrian situated 2 m away from the antenna, the wavefront curvature may introduce deviations.

From theoretical scattering to observed signatures. While the Sinclair matrix $\boldsymbol{S}$ provides a deterministic description of target scattering in an ideal environment, the transition to practical automotive sensing introduces two significant layers of complexity: hardware-induced distortion and the stochastic nature of distributed targets.

In practical scenarios, the measured matrix $\boldsymbol{M}$ is a transformation of the true scattering matrix $\boldsymbol{S}$ through the system's transfer functions. This is typically modelled as:[3]

$$\boldsymbol{M} = \boldsymbol{R}\boldsymbol{S}\boldsymbol{T} + \boldsymbol{C} + \boldsymbol{N}, \tag{2.6}$$

where $\boldsymbol{T}$ and $\boldsymbol{R}$ represent the polarimetric imbalances of the transmitter and receiver chains, $\boldsymbol{C}$ accounts for antenna mutual coupling and leakage, and $\boldsymbol{N}$ is the additive noise. Characterizing these terms is the primary objective of the calibration routines detailed in Chapter 6.

Second, in the presence of complex, non-point-like targets such as VRUs, a single Sinclair matrix is often insufficient to capture the depolarization caused by multiple scattering centres. This necessitates the use of the second-order statistics introduced in the following section.

2.1.3 Stokes parameters and the Poincaré sphere

In dynamic automotive scenarios, electromagnetic waves typically interact with *distributed scatterers* – extended targets such as road surfaces, vegetation, vehicles, or tunnel walls that

[1] When defining the polarimetric scattering matrix, it is necessary to assume a frame in which the polarization is defined. Generally, there are two principal conventions: the *forward scatterer alignment* (FSA) and the *backscatter alignment* (BSA). While the FSA convention, sometimes called *wave-oriented*, defines the polarization basis for both incident and scattered waves so that the Cartesian z-axis always faces the $\boldsymbol{k}$ direction, the BSA system operates by defining the basis of the scattered wave with respect to the receiving antenna. This text assumes the BSA convention, as is standard for monostatic radar. This choice simplifies the scattering definition by defining a fixed coordinate system for both the incident and backscattered waves relative to the antenna.

[2] Even after this reduction, fully polarimetric systems, capable of measuring the full scattering response, dispose of five independent parameters per resolution cell. This is in contrast to single-polarized systems, which measure only two, and it shows the increased complexity and information content of polarimetric measurements.

[3] In polarimetric calibration, the equation is commonly expressed 'backwards', that is, by equating the ideal scattering matrix to the measured one transformed by $\boldsymbol{R}$ and $\boldsymbol{T}$ as the *correction* matrices. Here, we express it in the *forward* direction to emphasize the measurement process, hence taking $\boldsymbol{R}$ and $\boldsymbol{T}$ as the *distortion* matrices.

comprise numerous independent scattering centers within a single resolution cell. Because these sub-reflectors contribute random phase and amplitude fluctuations, the resulting interference induces depolarization, rendering the reflected wave partially polarized or incoherent. To characterize these complex fields, the Stokes parameters are employed; they provide a phase-agnostic description of the wave's polarization state based on observable, time-averaged power measurements.

The transition from Jones formalism to Stokes parameters involves considering the Jones vector components as random processes, $E_H(t)$ and $E_V(t)$. Taking the time-averaged[4] outer product of the Jones vector with its Hermitian transpose yields the Hermitian positive semidefinite wave covariance matrix $\boldsymbol{J}$, often called the *coherency matrix*:

$$\boldsymbol{J} = \langle \boldsymbol{E}_J \cdot \boldsymbol{E}_J^{\dagger} \rangle = \begin{bmatrix} \langle |E_H|^2 \rangle & \langle E_H E_V^* \rangle \\ \langle E_V E_H^* \rangle & \langle |E_V|^2 \rangle \end{bmatrix}, \tag{2.7}$$

where $\langle \cdot \rangle$ denotes temporal averaging. To facilitate convenient description through matrix decomposition, group theory is often employed. Specifically, the formalism considers the SU(2) group basis consisting of the Pauli matrices:

$$\boldsymbol{\sigma}_0 = \begin{bmatrix} 1 & 0 \\ 0 & 1 \end{bmatrix}, \quad \boldsymbol{\sigma}_1 = \begin{bmatrix} 1 & 0 \\ 0 & -1 \end{bmatrix}, \quad \boldsymbol{\sigma}_2 = \begin{bmatrix} 0 & 1 \\ 1 & 0 \end{bmatrix}, \quad \boldsymbol{\sigma}_3 = \begin{bmatrix} 0 & -\mathrm{i} \\ \mathrm{i} & 0 \end{bmatrix}. \tag{2.8}$$

These matrices form a basis for decomposing the coherency matrix – a decomposition technique commonly known as the *Pauli decomposition*:

$$\boldsymbol{J} = \frac{1}{2} \sum_{i=0}^{3} g_i \boldsymbol{\sigma}_i = \frac{1}{2} \begin{bmatrix} g_0 + g_1 & g_2 - \mathrm{i} g_3 \\ g_2 + \mathrm{i} g_3 & g_0 - g_1 \end{bmatrix}. \tag{2.9}$$

Here, the coefficients g_i are the *Stokes parameters*, defined as $g_i = \mathrm{tr}(\boldsymbol{J}\boldsymbol{\sigma}_i)$. Together, they form the *Stokes vector* $\boldsymbol{g}$, expressed as:

$$\boldsymbol{g} = \begin{bmatrix} g_0 \\ g_1 \\ g_2 \\ g_3 \end{bmatrix} = \begin{bmatrix} \langle |E_H|^2 \rangle + \langle |E_V|^2 \rangle \\ \langle |E_H|^2 \rangle - \langle |E_V|^2 \rangle \\ 2\,\mathrm{Re}\langle E_H E_V^* \rangle \\ -2\,\mathrm{Im}\langle E_H E_V^* \rangle \end{bmatrix}. \tag{2.10}$$

As evident from Equation (2.10), the Stokes parameters are *real-valued power quantities* directly measurable via standard RF detectors. While the diagonal elements J_{pq} represent the intensities, the off-diagonal elements capture the complex cross-correlation between the horizontal and vertical components. Geometrically, the parameters g_1, g_2, g_3 span a three-dimensional orthogonal basis, mapping the polarization state onto the *Poincaré sphere*, as illustrated in Figure 2.1. Within this topological framework, the parameter g_0 represents the total wave intensity and corresponds to the radius of the sphere.

Consequently, the condition of physical realizability – derived from the positive semi-definiteness of the coherency matrix – requires that the state vector lies either on the surface or within the volume of the sphere:

$$g_0^2 \geq g_1^2 + g_2^2 + g_3^2. \tag{2.11}$$

The equality in Equation (2.11) holds strictly for fully polarized waves, which map to the sphere's surface. Conversely, the strict inequality characterizes partially polarized waves, which occupy the interior volume and are typical of clutter and distributed targets. This geometric distinction

[4]Taking the outer product of a single Jones vector $\boldsymbol{E}_J = [E_H, E_V]^{\mathrm{T}}$ without averaging would yield a rank-1 matrix, corresponding to the theoretical ideal of a fully polarized, perfectly coherent wave. Temporal averaging is essential to capture partial polarization effects.

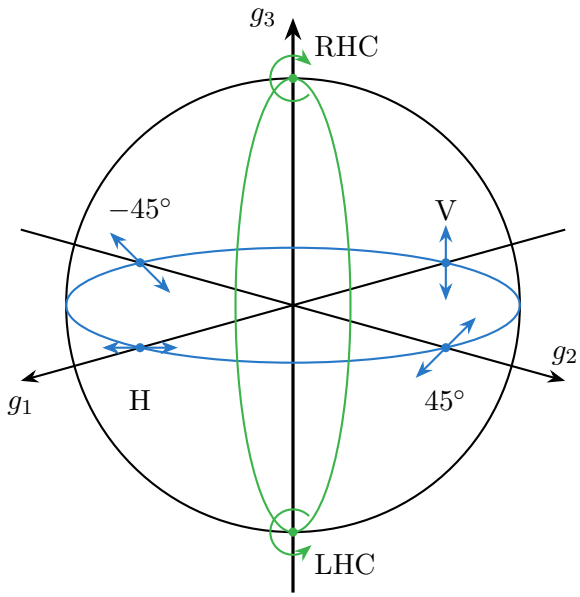

Figure 2.1: Representation of the polarization state on the Poincaré sphere. Fully polarized waves lie on the surface (DOP = 1), while partially polarized states lie within the volume (DOP < 1). The axes g_1, g_2, g_3 correspond to linear, linear-diagonal, and circular polarizations, respectively.

naturally leads to the definition of the *degree of polarization* (DOP) as the normalized radial distance from the origin:

$$\text{DOP} = \frac{\sqrt{g_1^2 + g_2^2 + g_3^2}}{g_0} = \sqrt{1 - 4\frac{\det(\boldsymbol{J})}{\text{tr}(\boldsymbol{J})^2}}. \tag{2.12}$$

This metric serves as a key discriminant between stable VRU scatterers and distributed clutter, a feature that will be exploited in later chapters Chapter 5 for target classification. By applying *polarimetric decompositions* to the coherency matrix $\boldsymbol{J}$, we can decouple the scattering into constituent mechanisms, such as single-bounce, double-bounce, and volume scattering. In the following sections, these decomposition theorems are utilized to extract robust polarimetric signatures, providing the feature set required for the classification models developed later in this work.

2.2 Polarimetric target decomposition

The Sinclair and coherency matrices derived in Section 2.1 contain the complete polarimetric information of a target. However, in their raw matrix form, they offer little direct insight into the physical geometry of the scatterer. *Target decomposition* theorems aim to invert this relationship, expressing the measured matrix as a linear combination of canonical scattering mechanisms – such as flat plates, dihedrals, or dipoles – thereby extracting semantic features for classification.

These methods are broadly categorized into *coherent decompositions*, which operate on the Sinclair matrix $\boldsymbol{S}$ of deterministic targets, and *incoherent decompositions*, which operate on the coherency matrix $\boldsymbol{J}$ (or $\boldsymbol{T}$) of distributed targets.

2.2.1 Coherent decomposition

For deterministic targets with negligible noise and spatial variation, such as a car chassis or a corner reflector, the scattering process is fully coherent. As described by Gaglione et al. [6],

a general coherent polarimetric decomposition of the Sinclair matrix $\boldsymbol{S}$ can be expressed as a linear combination of M elementary scattering mechanisms; that is,

$$\boldsymbol{S} = \sum_{m=1}^{M} c_m \boldsymbol{S}_m, \tag{2.13}$$

where $\boldsymbol{S}_m$ are the canonical scattering matrices, encoding the response of the m-th canonical object, and c_m are generally complex coefficients, including both amplitude and phase information of each scattering mechanism.

Add a section on canonical scatterers prior to this.

The most established framework for interpreting radar targets is the *Pauli decomposition*, which projects the Sinclair matrix onto a scaled basis of Pauli matrices, $\{\sqrt{2}\boldsymbol{\sigma}_i\}_{i=0}^{3}$, where $\boldsymbol{\sigma}_i$ are defined in Equation (2.8).[5] The resulting vector representation of the scattering matrix, $\boldsymbol{S}$, is referred to as the *Pauli scattering vector* $\boldsymbol{k}_P$:

$$\boldsymbol{k}_P = \frac{1}{\sqrt{2}} \begin{bmatrix} S_{\mathrm{HH}} + S_{\mathrm{VV}} \\ S_{\mathrm{HH}} - S_{\mathrm{VV}} \\ S_{\mathrm{HV}} + S_{\mathrm{VH}} \\ \mathrm{i}(S_{\mathrm{HV}} - S_{\mathrm{VH}}) \end{bmatrix} \equiv \begin{bmatrix} a \\ b \\ c \\ d \end{bmatrix}. \tag{2.14}$$

The primary advantage of this basis is that it provides a direct physical interpretation of elementary scattering mechanisms. Consequently, the squared magnitude of each Pauli component quantifies the contribution of a specific canonical mechanism to the total radar cross-section (RCS). Specifically:

- *Single-bounce:* $|a|^2/2$ corresponds to odd-bounce scattering, typically arising from spheres, flat plates, or trihedral reflectors. In an automotive context, this mechanism dominates returns from flat surfaces, such as walls or the rear of a vehicle.
- *Double-bounce:* $|b|^2/2$ corresponds to even-bounce scattering derived from dihedral structures. This is commonly observed in the corner-like features of a car (e.g., window frames and side mirrors) or the ground-wall interaction of a curb.
- *Cross-polar:* $|c|^2/2$ represents the cross-polarization energy induced by dihedrals or dipoles rotated by 45° around the radar line-of-sight.
- *Asymmetric:* $|d|^2/2$ accounts for asymmetric scattering mechanisms, which may arise from complex target geometries or non-reciprocal propagation effects.

In strict monostatic configurations, the principle of reciprocity applies, theoretically forcing the fourth component to zero; practically, it will contain noise or system artefacts. In the ideal scenario of $d = 0$, the Pauli vector reduces to a three-dimensional representation:

$$\boldsymbol{k}_P = \begin{bmatrix} a \\ b \\ c \end{bmatrix} = \frac{1}{\sqrt{2}} \begin{bmatrix} S_{\mathrm{HH}} + S_{\mathrm{VV}} \\ S_{\mathrm{HH}} - S_{\mathrm{VV}} \\ 2S_{\mathrm{HV}} \end{bmatrix}. \tag{2.15}$$

However, in the *quasi-monostatic* scenarios relevant to this work – where transmit and receive antennas are closely spaced but not co-located – the asymmetry term d remains non-negligible.

[5] The scaling factor of $\sqrt{2}$ ensures that the Euclidean norm of the target vector matches the Frobenius norm of the scattering matrix, thereby satisfying the requirement for 'total power invariance'. The same reasoning applies to the lexicographic basis discussed later.

Lexicographic basis An alternative representation frequently encountered in the literature is the *lexicographic basis*, which is a scaled canonical basis of $\mathbb{C}^{2\times 2}$:

$$\Phi_0 = 2\begin{bmatrix}1 & 0\\ 0 & 0\end{bmatrix}, \quad \Phi_1 = 2\begin{bmatrix}0 & 1\\ 0 & 0\end{bmatrix}, \quad \Phi_2 = 2\begin{bmatrix}0 & 0\\ 1 & 0\end{bmatrix}, \quad \Phi_3 = 2\begin{bmatrix}0 & 0\\ 0 & 1\end{bmatrix}. \tag{2.16}$$

This basis orders the target vector elements as $\boldsymbol{k}_L = [S_{\mathrm{HH}}, S_{\mathrm{HV}}, S_{\mathrm{VH}}, S_{\mathrm{VV}}]^{\mathrm{T}}$, which is the native format for many radar hardware interfaces and is convenient for certain matrix operations, such as system calibration, it lacks the direct physical interpretability of the Pauli basis.

Alternative decompositions While Krogager and Cameron proposed alternative coherent decompositions, such utilizing circular polarization to decompose targets into sphere, diplane, and helix components, the Pauli basis remains the standard for coherent preprocessing due to its orthogonality and computational efficiency.

2.2.2 Cloude-Pottier incoherent decomposition

In the context of VRU classification, targets are rarely simple point scatterers. A pedestrian, for instance, is a complex aggregate of limbs with varying orientations and materials, possibly moving within a single resolution cell, creating a *distributed target*.

To analyse such targets, it is necessary to move from the coherent vector $\boldsymbol{k}_P$ to the second-order statistics represented by the *Pauli coherency matrix* $\boldsymbol{T}$:

$$\boldsymbol{T} = \langle \boldsymbol{k}_P \cdot \boldsymbol{k}_P^{\dagger} \rangle. \tag{2.17}$$

Note that $\boldsymbol{T}$ is mathematically equivalent to the matrix $\boldsymbol{J}$ defined in Equation (2.7), but represented in the Pauli basis rather than the lexicographic basis. The most powerful tool for analysing $\boldsymbol{T}$ is the *Cloude-Pottier decomposition*, based on the eigenvalue expansion of the Hermitian matrix $\boldsymbol{T}$:

$$\boldsymbol{T} = \sum_{i=1}^{3} \lambda_i \boldsymbol{e}_i \boldsymbol{e}_i^{\dagger}, \tag{2.18}$$

where $\lambda_1 \geq \lambda_2 \geq \lambda_3 \geq 0$ are the real eigenvalues and $\boldsymbol{e}_i$ are the orthogonal eigenvectors. This expansion allows the definition of three key parameters that describe the randomness and mechanism of the scattering:

Polarimetric Entropy (H). Defined from the logarithmic probability of the eigenvalues $P_i = \lambda_i / \sum \lambda_k$, entropy measures the randomness of the scattering process:

$$H = \sum_{i=1}^{3} -P_i \log_3 P_i, \quad 0 \leq H \leq 1. \tag{2.19}$$

$H = 0$ indicates a single dominant mechanism (isotropic point target), while $H = 1$ indicates random noise or fully developed volume scattering (e.g., dense foliage or complex clutter).

Mean Alpha Angle ($\bar{\alpha}$). By parameterizing the eigenvectors, the angle α_i is extracted to identify the physical mechanism associated with the i-th eigenvalue. The mean angle is defined as $\bar{\alpha} = \sum P_i \alpha_i$:

- $\bar{\alpha} \approx 0°$: Surface scattering (road, car body).
- $\bar{\alpha} \approx 45°$: Dipole/Volume scattering (vegetation, potentially limbs).
- $\bar{\alpha} \approx 90°$: Double-bounce scattering (ground-wheel, curb).

Anisotropy (A). This parameter characterizes the relative importance of the second and third eigenvalues:

$$A = \frac{\lambda_2 - \lambda_3}{\lambda_2 + \lambda_3}. \tag{2.20}$$

For VRUs, these parameters form a distinctive feature space (the H/α plane). While a vehicle is a low-entropy target ($H < 0.3$), pedestrians typically exhibit moderate-to-high entropy due to their non-rigid body dynamics, allowing for separation from static clutter.

2.2.3 Simple polarimetric descriptors

While eigenvalue decompositions offer rigorous physical insight, their computational cost – requiring diagonalization for every cell in a range-Doppler map – can be prohibitive for real-time automotive embedded systems. Consequently, simpler ratio-based descriptors are often employed as lightweight features for detection algorithms.

Common descriptors adapted from meteorology include:

- **Differential Reflectivity (Z_{DR}):** The ratio of horizontal to vertical received power, $10\log_{10}(\langle|S_{\mathrm{HH}}|^2\rangle/\langle|S_{\mathrm{VV}}|^2\rangle)$. This aids in distinguishing vertically oriented targets (pedestrians) from horizontal ones.
- **Linear Depolarization Ratio (LDR):** The ratio of cross-polar to co-polar power, $10\log_{10}(\langle|S_{\mathrm{HV}}|^2\rangle/\langle|S_{\mathrm{HH}}|^2\rangle)$. High LDR is a strong indicator of complex geometry or irregular surfaces typical of VRUs.
- **Co-polar Correlation Coefficient (ρ_{hv}):** The magnitude of the correlation between HH and VV channels. Man-made targets typically exhibit $\rho_{\mathrm{hv}} \to 1$, while natural distributed targets exhibit lower correlation.

2.2.4 Gap analysis: Applicability to automotive scenarios

The decomposition techniques reviewed above were historically developed for *synthetic aperture radar (SAR)* and remote sensing, operating under assumptions of static scenes, far-field plane wave incidence, and high-altitude geometries (steep incidence angles).

Transferring these methods to the automotive domain introduces specific challenges:

1. **Grazing Incidence:** Automotive radars operate near the ground. At grazing angles, the Brewster angle effect can suppress vertical polarization returns from the road surface, artificially inflating Z_{DR} and distorting the α parameter.
2. **Coherent Integration Time:** In SAR, the integration time is long enough to form a well-defined covariance matrix. In dynamic automotive scenarios, the "target" (e.g., a cyclist) moves across range cells rapidly. Estimating $\boldsymbol{T}$ requires averaging over a window that assumes stationarity, a condition often violated by fast-moving VRUs.
3. **Micro-Doppler Coupling:** Standard decomposition ignores Doppler. For VRUs, the polarimetric signature is time-variant and coupled with the micro-Doppler signature (e.g., the swinging arm of a pedestrian has a different polarization response than the torso).

This suggests that while classical decompositions provide the *basis* for feature extraction, they must be extended to the joint Doppler-polarization domain – a topic underexplored in current literature and central to the processing framework proposed in this research.

2.3 Doppler-resolved polarimetric signatures

Goal of this section

- Motivation: Introduce time-varying and micro-Doppler effects that are lost when averaging over Doppler channels.
- Micro-Doppler and dynamic scattering: Discuss human gait, limb motion, bicycle rotation, etc., as examples of polarization-Doppler coupling.
- Joint angle-Doppler-polarization processing: Explain representation in multi-dimensional spaces (e.g., polarimetric time-frequency signatures).
- Current state of the art: Summarize recent developments in Doppler-resolved polarimetry, emphasizing underexplored dynamic analysis.
- Challenges: Data sparsity, synchronization, calibration drift, coherent alignment, and MIMO virtual array non-idealities.

2.4 Polarimetric MIMO processing for VRU classification

Goal of this section

- Conceptual integration: Outline how polarimetry and MIMO diversity jointly enhance target separability and classification robustness.
- Proposed framework:
  - Multi-channel coherent integration across polarization and spatial dimensions.
  - Feature-level fusion of Doppler-polarimetric descriptors.
  - ML/AI classification trends leveraging polarimetry (e.g., CNNs on Stokes-encoded spectrograms, transformer-based fusion).
- Illustrative use case: Application to vulnerable road user (VRU) classification – pedestrians, cyclists, scooters – emphasizing the unique polarimetric-Doppler micro-signatures.

2.4.1 Suitability for automotive radar

Automotive scenes differ fundamentally from the operating conditions assumed in polarimetric radar theory:

- Short range (5–60 m): transition region between near-field and far-field, invalidating plane-wave assumptions.
- High dynamics: scattering matrices evolve on millisecond timescales due to limb motion and ego-vehicle motion.
- Multipath dominance: ground reflections and vehicle surfaces introduce depolarization not predicted by classical models.
- Multiplexing constraints: sequential polarimetric switching increases Doppler ambiguity when combined with TDM-MIMO.

These discrepancies justify the development of *new polarimetric methods*, potentially including Doppler-resolved polarimetric processing and joint spatial-polarimetric feature extraction.

Notes

- Why polarimetric radar?
  - Weishaupt et al. [7]: 'In automotive applications, the additional information on the scattering process derived from polarimetry can be used for an improved classification of other road users [1], [2] or the enhanced perception of the static environment for localization purposes [3]. A typical new result through applying polarimetry is an estimate of whether an even or odd number of reflections occurred at a scatterer. This allows drawing conclusions on the object's geometries.'
  - …
- Major challenges [8]:
  - Increment of the cross-polarization level of the radiation pattern in off-broadside measurement
  - Varying antenna phase centres in MIMO polarimetric radar
  - Complexity of polarimetric radar calibration
  - Lack of comprehensive system model for joint development of antennas and calibration strategies

Bibliography

[1] J.-S. Lee and E. Pottier, *Polarimetric Radar Imaging: From Basics to Applications*. CRC Press, 19th Dec. 2017, 474 pp.

[2] J. F. Tilly, F. Weishaupt, O. Schumann, J. Dickmann and G. Wanielik, 'Road User Classification with Polarimetric Radars,' in *2020 17th European Radar Conference (EuRAD)*, Jan. 2021, pp. 112–115, DOI: 10.1109/EuRAD48048.2021.00039

[3] A. Tinti, S. Tejero Alfageme, S. Duque Biarge, J. Balcells-Ventura and N. Pohl, 'Fully Polarimetric Automotive Radar: Proof of Concept,' *IEEE Transactions on Radar Systems*, vol. 2, pp. 645–660, 2024, DOI: 10.1109/TRS.2024.3423631

[4] T. Visentin, *Polarimetric Radar for Automotive Applications*. KIT Scientific Publishing, 10th Apr. 2019, 188 pp.

[5] A. Zangwill. 'Modern Electrodynamics,' Cambridge Aspire website, Accessed: 20th Jan. 2026. [Online]. Available: https://www.cambridge.org/highereducation/books/modern-electrodynamics/E5448C70CBF3651B2056F28EBF859AE9

[6] D. Gaglione, C. Clemente, L. Pallotta, I. Proudler, A. De Maio and J. J. Soraghan, 'Krogager decomposition and Pseudo-Zernike moments for polarimetric distributed ATR,' in *2014 Sensor Signal Processing for Defence (SSPD)*, Sep. 2014, pp. 1–5, DOI: 10.1109/SSPD.2014.6943309

[7] F. Weishaupt, J. F. Tilly, N. Appenrodt, J. Dickmann and D. Heberling, 'Calibration and Signal Processing of Polarimetric Radar Data in Automotive Applications,' in *2022 Microwave Mediterranean Symposium (MMS)*, May 2022, pp. 1–6, DOI: 10.1109/MMS55062.2022.9825584

[8] C. Zhao, Y. Aslan and A. Yarovoy, 'Overview of Polarimetry in Application to Automotive Radar: Array Design, Calibration and Target Feature Extraction Concepts,' in *2025 19th European Conference on Antennas and Propagation (EuCAP)*, Mar. 2025, pp. 1–5, DOI: 10.23919/EuCAP63536.2025.10999201